







Free volume in the smectic-*E* phase of 4-hexyl-4' isothiocyanatobiphenyl studied by positron annihilation spectroscopy

E. Dryzek ¹, E. Juszyńska-Gałązka ¹, R. Zaleski ², B. Jasińska ², and M. E. S. Eusébio ³

¹*Institute of Nuclear Physics, Polish Academy of Sciences, 31–342 Kraków, Poland*

²*Institute of Physics, Maria Curie-Skłodowska University, Pl. M. Curie-Skłodowskiej 1, 20–031 Lublin, Poland*

³*CQC Departamento de Quimica, Universidade de Coimbra, Rua Larga 3004–534 Coimbra, Portugal*

 (Received 24 September 2019; revised manuscript received 21 November 2019; accepted 8 January 2020; published 26 February 2020)

Positron annihilation lifetime spectroscopy has been used to study 4-hexyl-4'-isothiocyanatobiphenyl. Changes of the orthopositronium lifetime parameters with temperature have been observed for the supercooled smectic-*E* phase. The measurements confirm that positronium is created and annihilates in a layer of a lower electron density containing alkyl chains of molecules. The two-state bond-lattice model of glass transition explains the thermal activation of the centers where orthopositronium is created and annihilates when the glass of the smectic-*E* phase softens. However, the subsequent cold crystallization of the softened regions also influences the orthopositronium lifetime and intensity, which complicates the picture seen by positrons. The measurements during isothermal crystallization suggest that it progresses in two stages. The first stage can be described by the Avrami equation with the Avrami exponent close to unity, which indicates low-dimensional crystallization. Similarly to liquid *n* alkanes, the application of pressure is equivalent to temperature lowering with the similar equivalence relationship between pressure and temperature, which seems to confirm the structure of the smectic-*E* phase with sublayers containing alkyl chains in a molten state. The dependence of the orthopositronium lifetime on pressure for the smectic-*E* phase may be described by the bubble model where the positronium bubble is approximated with a finite square potential well with the depth of $U = 1.45$ eV.

DOI: [10.1103/PhysRevE.101.022705](https://doi.org/10.1103/PhysRevE.101.022705)

I. INTRODUCTION

Thermotropic liquid crystals exhibit mesophases and phase transitions with a change in temperature. Their mesomorphic properties can be modified by changing the molecular length in a particular homologous series or by applying hydrostatic pressure. An example of such a homologous series is 4-*n*-alkyl-4'-isothiocyanatobiphenyls (*n*TCBs, *n* is the number of carbon atoms in the alkyl group), which have been a subject of research performed using a variety of measurement techniques to establish polymorphism and dynamic details [1–10]. For $n = 2–10$, *n* TCBs exhibit only one liquid crystalline phase, i.e., smectic-*E* phase (Sm-*E*) also called crystal *E* (Cry-*E*), which is the subject of our study. A new model of the Sm-*E* lamellar structure with two sublayers: the first one containing aromatic cores of molecules and the second one containing alkyl chains of molecules, was proposed by Saito *et al.* [11,12]. Our previous positron annihilation lifetime spectroscopy (PALS) measurements for 4TCB allowed us to confirm the applicability of this model of the molecular arrangement in the Sm-*E* phase [13,14]. An essential feature of the Sm-*E* phase is the molten state of the alkyl chains of molecules [15,16]. The sublayer of molten alkyl chains of molecules provide sites, where positronium (Ps), i.e., the hydrogenlike bound state of the positron and electron, can be formed. Ps with parallel particle spins, i.e., orthopositronium (o-Ps) is a very sensitive probe of local regions of reduced electron density such as vacancies and interstitial volumes in molecular crystals, or free volume

holes in amorphous phases [17]. This is due to the pick-off process, which causes that the o-Ps decays as the result of the annihilation of its positron with an electron of opposite spin from the surrounding medium. Therefore, o-Ps lifetime is related to the size of these free volume regions.

In recent years, PALS has been extensively utilized in studies of free volume characteristics in polymers but also low molecular weight glass formers [18–22]. Efforts are made to connect the temperature changes of the o-Ps lifetime with changes of structure and dynamics in such systems. This can shed light on the nature of the glass transition, which continues to be a subject of many studies performed for both low molecular weight liquids and polymeric melts. However, the phenomenon of glass formation in mesophases having partial long-range positional and/or orientational ordering of molecules is much less studied. Moreover, the majority of glass transition models concern only isotropic liquids. Against this background, the successful description of the positron annihilation characteristics versus temperature, obtained for quenched Sm-*E* phase of 4TCB, in terms of the two-state bond-lattice model of glass transition seems to be an important novelty [14,23].

The basis of the model implementation is the assumption that in the supercooled Sm-*E* phase, alkyl chains of molecules can form two types of domains: liquidlike in the viscoelastic state, and solidlike in the rigid state. Positronium (Ps) can be formed only in the liquidlike domains where mobility of alkyl chains is high enough. An additional assumption that the intensity of o-Ps is proportional to the fraction of

liquidlike domains is made. This allowed us to determine the equilibrium temperature, which is considered as the melting point of the solidlike domains, and the creation enthalpy of sites where Ps is formed and annihilates. The equilibrium temperature coincides with the temperature of the exothermic effect detected in the heat capacity dependence for quenched 6TCB [24].

This work aims to check whether the two-state bond-lattice model of glass transition can be applied to describe PALS results for the member of the n TBC homologous series with six carbon atoms in alkyl chain: 6TCB. The glass transition was observed for this compound using various experimental methods: infrared spectroscopy, polarized microscopy, and x-ray diffraction [9]. The parameters obtained from the dependencies of o-Ps lifetime and intensity can be compared with the glass transition temperature estimated using those methods. No less valuable is a detailed insight into the arrangement of molecules in the Sm- E phase of 6TCB taking into account the newest analysis of molecular packing in orthogonal smectic liquid crystals performed recently by Yamamura *et al.* [25]. Detailed understanding of molecular arrangement in the Sm- E phase is essential considering potential applications of liquid crystals exhibiting this phase as self-organizing molecular semiconductors for development of field effect transistors (OFETs) [26]. There have also been reported the induced Sm- E or smectic- B (Sm- B) phases composed of binary mixtures of charge-transfer liquid crystal substances though neither of the constituents exhibits highly ordered smectic phases. Such induced smectics also attract interest as candidates for materials used as organic semiconductors [27].

In this paper, we also present the results of the PALS measurements of 6TCB at elevated pressure. Since this type of studies is rather limited, we compare the obtained results with the high-pressure PALS results for liquid n alkanes taking into account that Ps forms in the sublayer containing molten alkyl chains of molecules [28–30].

II. EXPERIMENTAL DETAILS

The 6TCB compound was synthesized according to Ref. [1] at the Institute of Chemistry, the Military University of Technology in Warsaw. Positron lifetime spectra were measured using a standard fast-slow delayed coincidence setup with BaF₂ scintillation detectors. The resolution function was a single Gaussian with a full width at half maximum (FWHM) equal to 245 ps. The positron source of activity of 0.5 MBq enclosed in an 8- μ m Kapton foil was sandwiched between two samples of 6TCB and placed in the measurement chamber. In the chamber, the air pressure was maintained at the level of 0.5 Pa. Before starting measurements, the sample-source sandwich was kept in the chamber at 315 K for 48 h to ensure that the sample is in the Sm- E phase. The measurements were performed in the temperature range between 95 and 325 K. The PALS spectra measured for 3 h contained more than 2×10^6 counts. To register changes with time, in some cases three spectra were measured for 1 h each at the same temperature. All the spectra were analyzed using the LT 9.2 program [31]. Several measurement procedures were performed: on heating of the sample after fast cooling (average 3 K/min, maximum 7 K/min) from 315 to 95 K, on

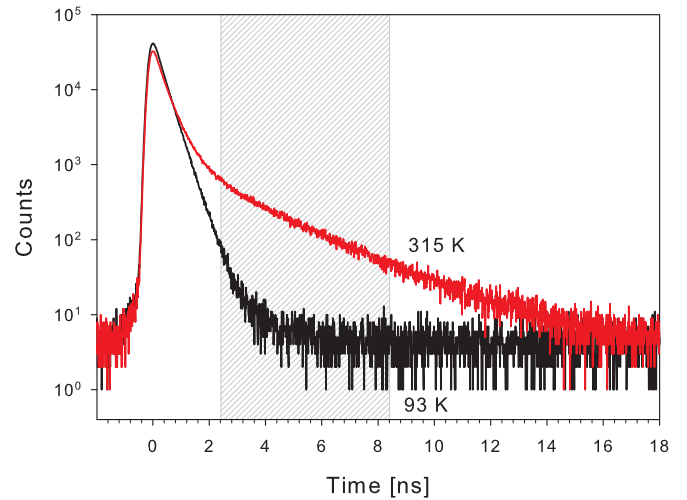


FIG. 1. Positron lifetime spectra for the Sm- E phase of 6TCB at 95 K (red) and 315 K (black). The hatched area shows the time range between 2.2 and 8.2 ns, where the main contribution to the spectrum comes from the o-Ps annihilation.

heating of the sample after slow cooling (constant 0.3 K/min), on heating with prolonged annealing of the sample between 245 and 275 K, and on cooling of the sample.

Only one positron lifetime component coming from positron annihilation in a free state was resolved in the spectra for temperatures lower than 150 K. For higher temperatures, the spectra consisted of three exponential components convoluted with the instrumental resolution curve and constant random coincidence background. The shortest-lived component was ascribed to parapositronium (p-Ps) decay, the intermediate one to the annihilation of free positrons, and the longest-lived one to o-Ps decay mostly due to the pick-off process. Figure 1 depicted the spectra registered at 315 K and 95 K after fast cooling of the sample. The time range between 2.2 and 8.2 ns was used for summing up the number of counts for the spectra registered for a short time (3 min.) in cases when fast changes were expected. The number of counts obtained in this way is approximately proportional to the intensity of o-Ps as it was discussed in Ref. [13].

The high-pressure PALS measurements were performed using the high-pressure chamber coupled with the Unipress U-11 compressor, which uses argon as a working gas. The positron source was sandwiched between two pellets of the measured material and placed in a small tube closed by two pistons sealed with o-rings. After closing the tube from one side, the air was evacuated from it and then, under vacuum, the second piston was slid into the tube in such a way that the pellets filled the whole volume between the pistons. After placing the tube in the chamber of the compressor, the pressure was applied to the sample via the pistons that were pressed by argon. In consequence, the sample had no contact with the gas during the measurement.

III. RESULTS AND DISCUSSION

The main discussion of the results concerns the behavior of the o-Ps lifetime τ_3 and its intensity I_3 . The obtained

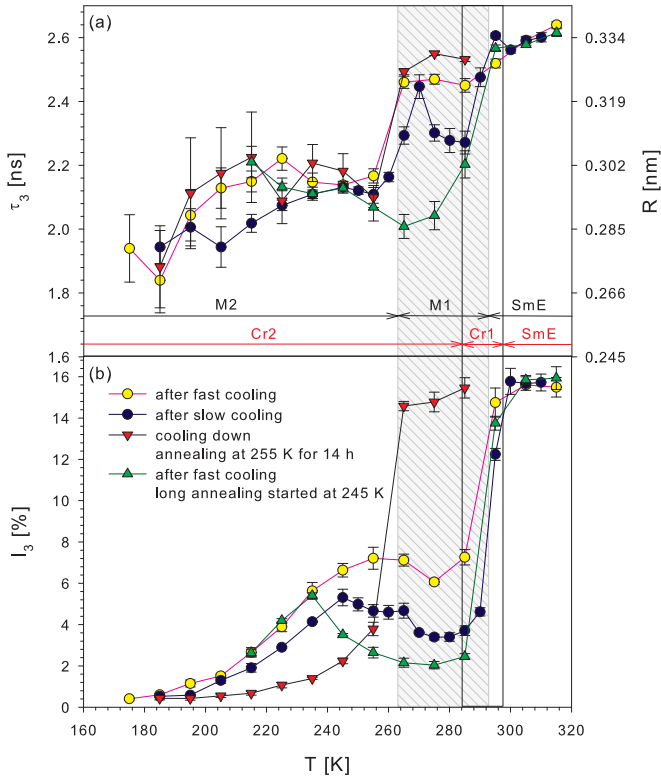


FIG. 2. Temperature dependencies of (a) τ_3 and (b) I_3 for four different measurement procedures. The right vertical axis shows the values of the free volume radius R calculated from Eq. (1).

dependencies of these quantities on temperature for 6TCB measured according to different procedures described above are shown in Fig. 2. On the right axis, there is depicted the radius R of the local free volume obtained from the Tao-Eldrup model [32,33]:

$$\tau_3 = \frac{1}{2} [1 - R/(R + \Delta R) + (1/2\pi) \sin(2\pi R/(R + \Delta R))]^{-1}, \quad (1)$$

where $\Delta R = 0.166$ nm is a parameter related to the penetration of the o-Ps wave function into the hole walls and was determined empirically.

A. Measurement on heating of the sample after fast cooling

For the sample of 6TCB after fast cooling from the Sm-*E*, the o-Ps component appears at 175 K. Its intensity is lower than 1% and increases reaching a local maximum of 7.2% at 255 K as shown in Fig. 2(b) (light color circles). The significant increase takes place at 295 K. This temperature is close to the melting temperature of the metastable crystal phase M1, i.e., 294 K [9]. An increase in τ_3 value at 295 K is also visible in Fig. 2(a), but it is small. A more noticeable increase in τ_3 value can be seen at 265 K, which is close to the transition temperature between two metastable phases M2 and M1, i.e., 264 K [9]. The behavior of I_3 for quenched Sm-*E* phase of 6TCB differs from that previously observed for 4TCB, which had a well-defined sigmoidal character. A steep increase in I_3 and τ_3 was observed only for melting of the molecular crystal phase of 4TCB [13]. Therefore, one can

conclude that the sample of 6TCB fast cooled from the Sm-*E* phase at least partially crystallizes on heating.

For 4TCB, the sigmoidal shape of the I_3 dependence on temperature was not disturbed by crystallization because the crystallization of 4TCB is much more difficult. The temperature dependence of o-Ps component intensity for 4TCB was described using the bond-lattice model of glass transition [14,23]. The model assumes that the molecules occupy one of the two thermodynamic states: solidlike or liquidlike regarding the mobility of their alkyl chains. At a certain temperature, molecules form two types of domains: liquidlike in the viscoelastic state, and solidlike in the rigid state. In liquidlike domains, the mobility of alkyl chains is high enough for Ps to form a bubble and then annihilate in the pick-off process [34]. Vitrification of the Sm-*E* phase consists in the freezing of the alkyl chain motions; thus, Ps does not form at a low temperature. The thermally activated creation of the sites where o-Ps forms and annihilates in the quenched Sm-*E* phase of 4TCB is reflected in the sigmoidal shape of the I_3 temperature dependence.

For 6TCB, vitrification of Sm-*E* phase was observed by Jasiurkowska *et al.* [9]. Polarization microscopy revealed appearing of cracks in the texture of the Sm-*E* phase at low temperatures and their disappearing on heating. The growth of the smectic layer spacing by 0.4 Å in the vicinity of 200 K was explained by softening of the glass, and 175 K was indicated as the glass transition temperature. This temperature corresponds well with the temperature at which o-Ps component becomes visible in the lifetime spectra. Because of the low intensity, the o-Ps lifetimes are determined with high uncertainties in this region, but some increase in τ_3 , which coincides with the increase in the smectic layer spacing, is visible.

Figure 3 presents the dependencies of the o-Ps lifetime and intensity for the sample after fast cooling when three spectra were registered for 1 h at each temperature. Up to 225 K, the values of I_3 does not change within the triplets. However, starting from 235 K up to 285 K, the increase in temperature results in an increased value of I_3 for the first spectrum registered caused by the increase in the fraction of molecules in the liquidlike state. For the next two spectra registered at the same temperature, the value of I_3 decreases, which indicates that the fraction of molecules in the liquidlike state diminishes. The domains, which previously have converted from the solidlike to the liquidlike state, can crystallize. As was observed for 4TCB, crystallization causes a decrease in o-Ps lifetime intensity because in that case, o-Ps can form only in open volume imperfections of a crystal lattice such as molecular vacancies.

Cold crystallization of a small molecule glassformer, salol (phenyl salicylate), was observed in PALS experiments by Dlubek *et al.* [35]. It also manifested itself as a substantial decrease in the Ps formation connected to the decrease in I_3 since the crystalline salol shows no Ps formation. Therefore, it may be concluded that on cooling, a glassy state of the Sm-*E* phase is formed. Then on heating at 175 K softening of the glass begins, which is followed by crystallization of a metastable phase starting at 235 K. Transition from the metastable phase M1 to M2 is connected to the increase in the radius of the open volume from 2.9 Å to 3.2 Å [Fig. 2(a)].

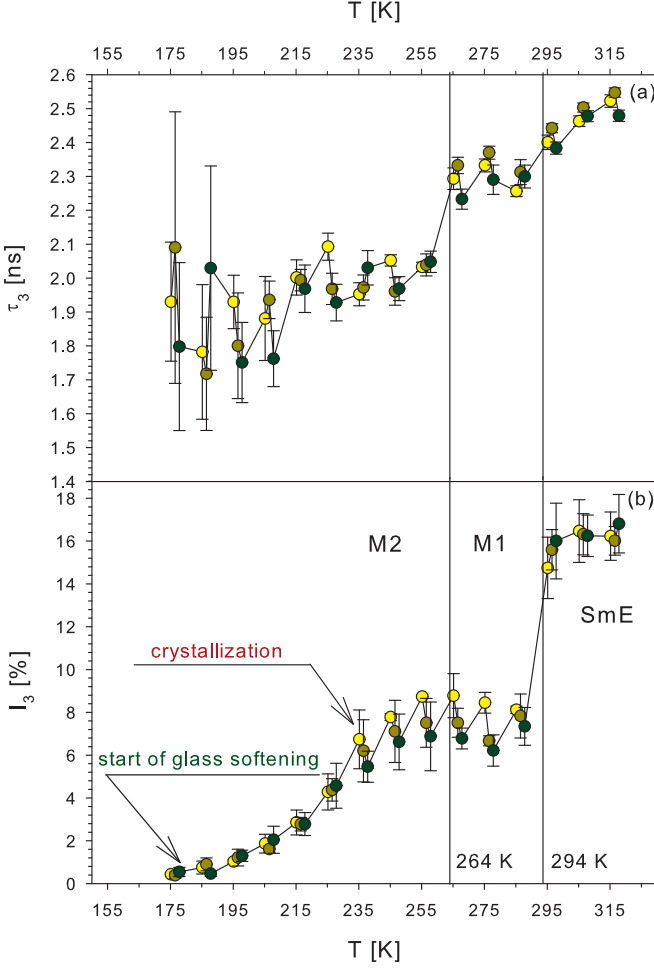


FIG. 3. Temperature dependencies of (a) τ_3 and (b) I_3 for the sample after fast cooling from the Sm-E phase. The triplets of points were obtained from the three spectra registered for 1 h each without changing the sample temperature.

In this analysis, the open volume radius is treated as a mean value because, depending on the temperature, the sample may be a mixture of domains in a vitreous state, a liquidlike state, and one or more molecular crystal polymorphs. At 294 K the metastable phase M2 melts to the Sm-E phase and open volume radius increases to 3.3 Å at 195 K, which is accompanied by a significant increase in I_3 [Fig. 2(a)]. Then o-Ps lifetime continues to increase slightly, which may be caused by the thermal expansion related to the further increase in the smectic layer spacing above the transition temperature [9].

In order to compare the changes in the intensity of the o-Ps component with temperature for 6TCB and 4TCB, both dependencies are shown in Fig. 4. The dependence for 4TCB is taken from Ref. [14]. The solid line is fitted according to the bond-lattice model of glass transition, in which the liquidlike fraction of the sample, η_{liq} , is given by the equation:

$$I_3(T) = A\eta_{\text{liq}}(T) = \frac{A}{1 + \exp\left[\frac{H}{T}\left(1 - \frac{T}{T_e}\right)\right]} \text{ (in\%)}, \quad (2)$$

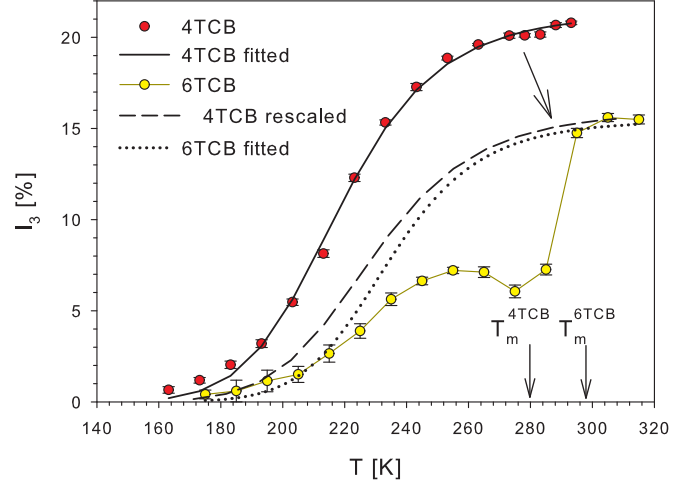


FIG. 4. Temperature dependencies of I_3 for 6TCB and 4TCB. The dependence for 4TCB is taken from Ref. [14]. The solid line was fitted to the experimental points using Eq. (2). The dashed line is obtained by rescaling the solid line for 4TCB by the ratio of the melting temperatures to the Sm-E phase $T_m^{6\text{TCB}}/T_m^{4\text{TCB}}$ and the ratio of the o-Ps component intensity $I_3^{6\text{TCB}}/I_3^{4\text{TCB}}$ for the Sm-E phase above the melting temperature. The dotted line is a fit of Eq. (2) to the experimental points for 6TCB for temperatures up to 215 K and then above the transition temperature to the Sm-E phase.

where $H = h_b z_{\text{eff}}/k_B$, h_b is the energy difference per closed bond, z_{eff} is the effective coordination number of the first shell, and k_B is Boltzmann's constant, T_e is the equilibrium temperature between the solidlike and liquidlike domains. To reduce the number of adjustable parameters, we assume that for $\eta_{\text{liq}} = 0$, $I_3 = 0$. For $\eta_{\text{liq}} = 1$, we assume that I_3 is an average of the values obtained for the Sm-E phase just above the transition from the molecular crystal phase, which gives the constant A . For 6TCB, $A = I_3^{6\text{TCB}} = (15.7 \pm 0.1)\%$.

The dependence for 4TCB is then rescaled by the ratio of the transition temperatures to the Sm-E phase $T_m^{6\text{TCB}}/T_m^{4\text{TCB}}$ and the ratio of the o-Ps component intensity $I_3^{6\text{TCB}}/I_3^{4\text{TCB}}$ for the Sm-E phase above the melting temperature. The obtained dependence is shown as a dashed line in Fig. 4. Parameters of the bond-lattice model of glass transition obtained for 6TCB from the rescaled curve are the following: $H = 3127$ K and $T_e = 229$ K. They are higher than those for 4TCB: $H = (2980 \pm 133)$ K and $T_e = (219 \pm 1)$ K, which results from the higher melting temperature of $T_m^{6\text{TCB}}$.

Assuming that $I_3(T)$ dependences in both 4TCB and 6TCB should have the same shape after rescaling, the differences indicate that the influence of crystallization lowers I_3 and thus the liquidlike fraction already at 205 K. However, in Fig. 3 this influence is visible only above 225 K and in Fig. 5, which is analyzed below, it is clearly visible above 215 K. Fitting the model only to the points for temperatures up to 215 K and then above the transition temperature to the Sm-E phase gives the dotted curve in Fig. 4. The values of the parameters are slightly higher than those from the rescaling: $H = (3685 \pm 398)$ K and $T_e = (238 \pm 3)$ K. The enthalpy per 1 mol of excitations, i.e., per 1 mol of created o-Ps annihilation sites, is only slightly higher in 6TCB in comparison to 4TCB. If we take into account both curves from Fig. 4, it changes

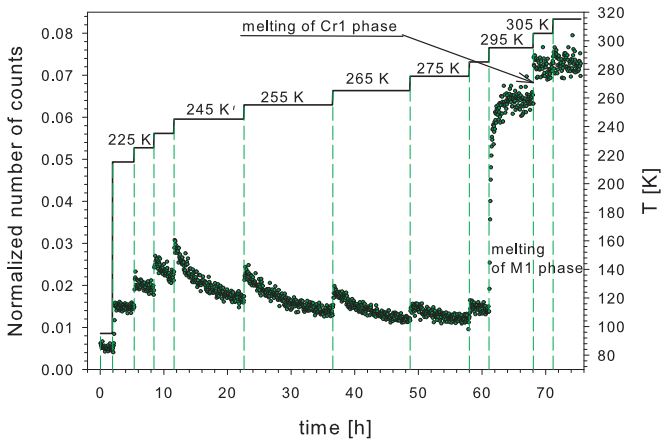


FIG. 5. The normalized number of counts between 2.2 and 8.2 ns calculated from the spectra registered in 3 min intervals as a function of time for the measurement on heating of the sample after fast cooling with longer annealing stages between 245 and 275 K. The dependencies of τ_3 and I_3 for this measurement is depicted in Fig. 2 (triangles up). The temperature is shown on the right axis.

from $24.8 \pm 1.1 \text{ kJ mol}^{-1}$ for 4TCB to $26\text{--}31 \text{ kJ mol}^{-1}$ for 6TCB. The entropy changes from $113 \pm 1 \text{ J mol}^{-1}\text{K}^{-1}$ for 4TCB to $118\text{--}123 \text{ J mol}^{-1}\text{K}^{-1}$ for 6TCB.

Instead of a typical step in the heat capacity ΔC_p at the glass transition temperature T_g , the bond-lattice model predicts a different character of the configurational heat capacity dependence $C_p(T)$, which can be described as an asymmetrical hump-like rise with a maximum at T_e [36]. This type of behavior was observed for the quenched Sm-*E* phase of 4TCB and described as a hump between 150 and 250 K [24]. Similar hump is also visible for the quenched Sm-*E* phase of 6TCB, but there are also superimposed two anomalies: the first one at 264 K, which is identified as a solid-to-solid phase transition between M2 and M1 phases, and the second one at 294 K, which appears due to the phase transition from M1 phase to the Sm-*E* phase [9].

The additional measurement with longer annealing stages between 245 and 275 K was performed on heating after fast cooling of the sample from the Sm-*E* phase. During this measurement, the PALS spectra were registered in 3 min intervals. The normalized number of counts in the time interval between 2.2 and 8.2 ns since a positron birth (shown in Fig. 1) as a function of the measurement time is depicted in Fig. 5. The temperature of the sample is also shown (right axis). The temperature rise of 10 K causes a sharp increase in the number of counts connected to the glass softening. Starting from 225 K, the number of counts decreases when the sample is kept at a constant temperature, which indicates crystallization. Transition to the Sm-*E* phase takes place in two steps. The increase in the number of counts at 295 K indicates the melting of the metastable phase M1. The second much smaller increase at 305 K indicates that a part of the sample was in the Cr1 phase which melts at 304 K. Dependencies of o-Ps lifetime and intensity for this measurement are shown in Fig. 2 (triangles up). Both quantities exhibit the lowest values in the temperature range of the metastable phase M1, i.e., before the transition to the Sm-*E* phase. This suggests that the molecules

are more densely packed. The o-Ps lifetime of 2.0 ns in 6TCB close to the transition to the Sm-*E* phase is slightly higher than in the case of 4TCB molecular crystal [13].

B. Measurement on heating of the sample after slow cooling

After slow cooling of the sample that was initially in the Sm-*E* phase, the o-Ps component appears ($I_3 > 0$) at the temperature higher by 10 K than for the sample after fast cooling (Fig. 2, closed circles). Its intensity is lower than for the sample after fast cooling up to transition temperature to the Sm-*E* phase. We explain this as follows: a part of the sample has crystallized already on cooling while another part has formed a vitreous state of the Sm-*E* phase. The initial increase in I_3 indicates softening of the glass. The decrease in I_3 above 245 K indicates crystallization of regions, which transformed to the liquidlike state. It is worth noticing that there is a steplike decrease in I_3 at the transition temperature between metastable phases M2 and M1. The lifetime τ_3 also increases initially similarly to the sample after fast cooling described above (light color circles in Fig. 2). This behavior, together with the low values of I_3 , indicates a more ordered structure, i.e., one with less crystal lattice imperfections of a larger size. Then, above 270 K, τ_3 decreases, which means that the mean-free volume radius calculated according to Eq. (1) decreases to 3.1 Å. Thus crystal lattice imperfections are smaller. However, in the region of Cr1 occurrence, τ_3 again increases to the values characteristic for the Sm-*E* phase. There is visible a two-step increase in I_3 : the first step pointing out melting of the metastable phase M1 (on the border of the dashed area denoting the M1 phase temperature range in Fig. 2) and the second step pointing out melting of the molecular crystal Cr1 (on the border between the Cr1 and the Sm-*E* phase) [9]. Therefore, before melting to the Sm-*E* phase, the sample was a mixture of the M1 and Cr1 phases.

C. Measurement on cooling and crystallization

When the sample is cooled from the Sm-*E* phase, the o-Ps lifetime and intensity decrease initially only slightly. They both decrease significantly only at 255 K, i.e., below the temperature of transition between metastable phases M1 and M2 (Fig. 2, triangle down). The sample was kept at this temperature for 13.2 h. Figure 6 shows the normalized number of counts between 2.2 and 8.2 ns calculated for the spectra registered at 3 min intervals as a function of the measurement time. It can be seen that the number of counts, which is approximately proportional to I_3 , starts to decrease as soon as the sample temperature is lowered to 255 K. The data for the measurement at 255 K is summed in the 1 h spectra. The intensity and lifetime of o-Ps component obtained from the analysis of these spectra are shown in Fig. 7. The decrease in I_3 or normalized number of counts at 255 K indicates a decrease in the liquidlike fraction of the sample due to crystallization. The value of I_3 reaches a plateau at about 4% after approximately 10 h. Let us assume that after this time the sample transforms entirely to the M2 phase and the volume fraction of M2 phase, x , is proportional to the intensity I_3 as follows: $x = aI_3 + b$, where $a = -10.53$ and $b = 14.59$ are constants. Then we can perform the analysis similar to that

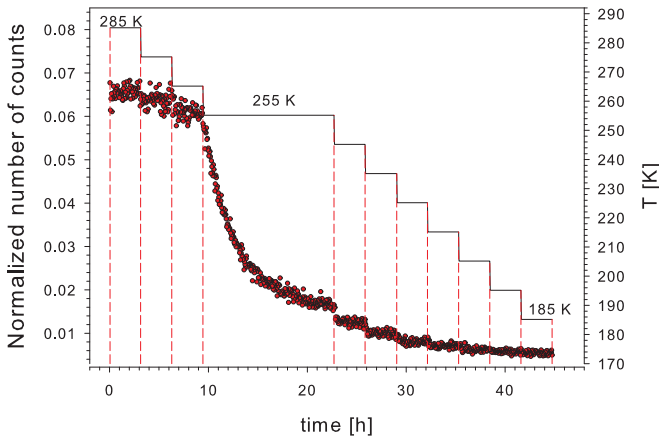


FIG. 6. The normalized number of counts between 2.2 and 8.2 ns calculated from the spectra registered in 3 min intervals as a function of time for the measurement on cooling of the sample with a more extended annealing stage at 255 K. The dependencies of τ_3 and I_3 for this measurement are depicted in Fig. 2 (triangles down). The temperature is shown on the right axis.

implemented for crystallization of 4TCB [13]. The inset in Fig. 7 shows log-log plot obtained from I_3 dependence on time and the fitted Avrami dependence $\log[-\ln(1-x)] = n \log(t) + \log k$, where n is the Avrami exponent, and k is the rate constant. The parameters obtained from the fit are the following: $n = 1.27 \pm 0.03$, $k = (6.3 \pm 1.6) \times 10^{-6} (\text{s}^{-n})$, $\tau_{cr} = k^{-1/n} = (1.2 \pm 0.2) \times 10^4$ s. For 4TCB, the Avrami exponent

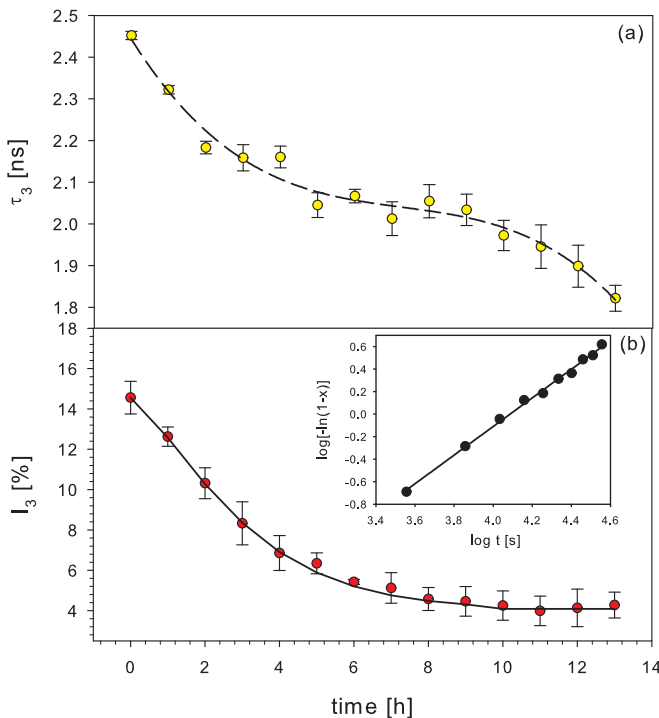


FIG. 7. Temperature dependencies of (a) τ_3 and (b) I_3 from the spectra registered for 1 h when the sample was kept at 255 K. The normalized number of counts for this measurement is shown in Fig. 6. The inset shows log-log plot obtained from I_3 dependence on time and the fitted Avrami equation.

$n = 1.73$. For 6TCB, it is lower and close to unity. Therefore, we conclude that there are some differences in the crystallization of these two compounds, but in both cases, a low-dimensional crystallization occurs. The more than seven times shorter crystallization time τ_{cr} for 6TCB in comparison to 4TCB is consistent with the fact that crystallization of the Sm-*E* phase of 4TCB, which started after 48 h incubation, took about 90 h. However, the dielectric relaxation measurements indicated that the crystallization of Sm-*E* phase of 6TCB could be described by two Avrami processes with exponents lower than unity [37].

The closer inspection of the o-Ps lifetime dependence shows that initially it behaves similarly to the I_3 dependence, i.e., after an initial decrease it reaches a plateau at about 2.05 ns, but after 10 h it starts to decrease again. Further changes in the sample are connected to a decrease in the mean radius of local free volume holes. That may be explained as follows: In the first stage, the sample crystallizes to the metastable phase M2, which, after that, starts to transform into a more stable crystal phase [9].

D. Positronium and the arrangement of molecules in the Sm-*E* phase of 6TCB and 4TCB

The newest research reported by Yamamura *et al.* clarifies the molecular packing mode in the orthogonal smectic liquid crystals [25]. Therefore, the PALS results should be analyzed taking into account those findings. According to them, biphenyl moieties of the n TCB molecules arranged antiparallelly in pairs fully overlap each other as shown in Fig. 8(a). They form highly ordered core layers. The isothiocyanate group ($-\text{N}=\text{C}=\text{S}$) of one molecule in the pair is located besides a part of the alkyl chain of the second molecule called the core-side chain. The isothiocyanate groups, which are bend at their N atom, together with the core-side chains form the thin core-side layer. The ends of the disordered alkyl chains, which conformations change dynamically, constitute the pure chain layer. The chain layer comprises the pure chain layer and two side-chain layers.

Figure 8 shows the layered structure of the Sm-*E* phase of 6TCB [Fig. 8(b)] and 4TCB [Fig. 8(c)] and the Ps bubble. The thickness of the core layer equals to the average distance between C1 and C1' in the adjacent antiparallel molecules. The thickness of the chain layer corresponds to the double average length of the conformationally disordered chains. Both quantities calculated using Eqs. (1) and (2) from Ref. [25] for 6TCB and 4TCB are shown in Fig. 8. As it was previously analyzed for 4TCB, Ps can form in the regions of the lower electron density, i.e., the layer of alkyl chains [14]. If we assume that the thickness of the side-chain layer is similar to the increment of the smectic layer spacing per CH_2 group equal to 1.4 Å we obtain the thickness of the pure chain layer close to 8.4 Å for 6TCB and 5.6 Å for 4TCB. It can be seen that for 6TCB, the Ps bubble diameter is distinctly smaller than the thickness of the chain layer. For 4TCB it is comparable with the estimated thickness of that layer. It is interesting that the Ps bubble for 6TCB does not occupy the whole available thickness of the chain layer. This situation can be compared with that in liquid n alkanes. For longer chains, starting from $n = 6$, Ps interacts only with short segments of

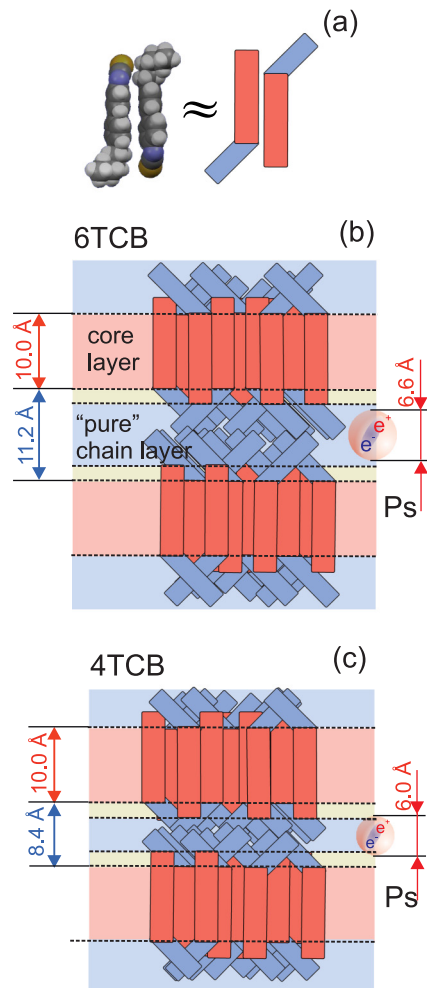


FIG. 8. Schematic illustration of (a) the antiparallel pair of 6TCB molecules and molecular arrangement in the Sm-*E* phase proposed in Ref. [25]: for (b) 6TCB and (c) 4TCB. The core chain layer contains biphenyl moieties, which fully overlap each other in the antiparallel pairs of molecules. Its thickness is equal to the average distance between C1 and C1' in the adjacent antiparallel molecules. The chain layer contains the ends of the disordered alkyl chains, which conformations change dynamically. The pure chain layer together with two layers containing isothiocyanate groups ($-\text{N}=\text{C}=\text{S}$) and parts of the alkyl chain adjacent to the biphenyl moieties form the chain layer. The estimated thickness of the core and chain layers and the size of the Ps bubble are shown.

chains regardless of the chain length and the diameter of the Ps bubble does not depend on the number of carbon atoms in the whole chain [38]. In case of 6TCB, steric conditions for longer alkyl chains of molecules whose at least C1 atom has a specific location can play a role.

There is also a difference in the intensity of o-Ps between 6TCB and 4TCB. The ratio of the o-Ps component intensity for the Sm-*E* phase of 6TCB and 4TCB, $I_3^{6\text{TCB}}/I_3^{4\text{TCB}}$, is equal to 0.76 even though the volume fraction of the alkyl chain layer for 6TCB (about 0.4) is higher than that for 4TCB (about 0.3). The intensity ratio $I_3^{6\text{TCB}}/I_3^{4\text{TCB}}$ seems to coincide with the reciprocal ratio of the volume fractions of the pure chain layers, i.e., 0.75.

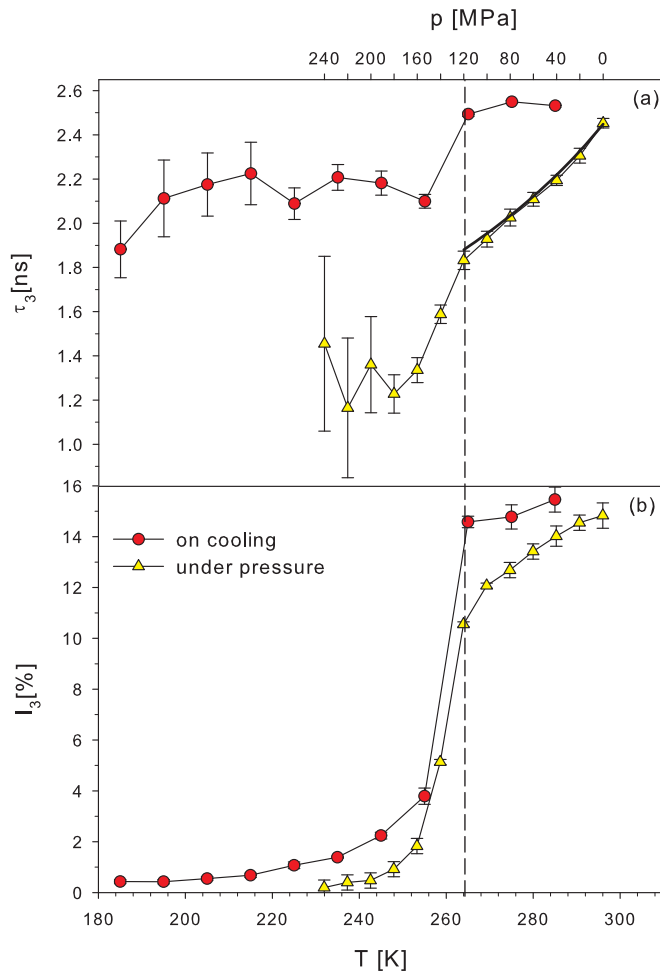


FIG. 9. The dependencies of (a) τ_3 and (b) I_3 on pressure plotted against the upper axis and dependencies of (a) τ_3 and (b) I_3 on the temperature measured on cooling of the sample, taken from Fig. 2. The solid line was obtained by calculating the Ps energy approximating the bubble with a finite square potential well of a spherical geometry with the depth $U = 1.46$ eV.

E. Measurement under high pressure

The dependencies of the o-Ps lifetime and intensity on the applied pressure are plotted against the upper axis in Fig. 9. In the same figure, there are also shown the dependencies of the o-Ps lifetime and intensity on temperature taken from Fig. 2 measured on cooling of the sample. To compare the results of these two experiments, we assume that, similarly to *n* alkanes, the application of pressure is equivalent to a temperature lowering [28,39]. Basing on this assumption, the steplike decrease in the intensity of o-Ps component at 120 MPa can be ascribed to the transition from the Sm-*E* phase to the metastable phase M2, which at low pressure takes place at 264 K. The transition is also marked by a change in the slope of the τ_3 dependence to a more steep one. The o-Ps lifetime decreases monotonically starting already at 20 MPa as a result of the increasing contribution of the external pressure to the equilibrium energy of the Ps bubble. Before the transition, the o-Ps lifetime decreases to 1.83 ns. It eventually reaches the value of c.a. 1.2 ns at 160 MPa for the sample presumably

in the metastable phase M2. It is much smaller than the value obtained when this phase is reached by the lowering of the temperature. The intensity of o-Ps is also lower for the sample under high pressure.

The PALS measurements under high pressure for liquid n alkanes reported by Goworek and Zgardzińska confirmed that for these compounds, the temperature decrease by 1 K is equivalent to the pressure increase by approximately 4 MPa [29]. The relationship obtained for 6TCB is similar: 1 K is equivalent to approximately 3.8 MPa, which is understandable, taking into account that alkyl chains are the nonrigid parts of molecules. This coincidence is an additional argument in favor of the nanosegregation of the molecule parts in the Sm- E phase and the presence of a sublayer containing alkyl chains in a molten state. However, the obtained dependencies of the o-Ps lifetime on temperature and pressure do not overlap to such a degree as it takes place for liquid n -alkanes [30].

The size of the Ps bubble in a liquid can be calculated using the bubble model [34]. The radius of the spherical bubble, R , is determined by minimizing the energy of the Ps-liquid system

$$\frac{\partial}{\partial R} \left[E_{Ps}(R) + 4\pi R^2 \sigma + \frac{4}{3} \pi R^3 p_{\text{ext}} \right] = 0, \quad (3)$$

where E_{Ps} is the zero-point energy of Ps in the potential well, σ is the surface tension, and p_{ext} is the external pressure. Commonly, E_{Ps} is calculated for the well-established approximation used in the Tao-Eldrup model, i.e., the infinite potential well broadened by $\Delta R = 0.166$ nm [32,33]. The external pressure is known from the measurement; thus, the only unknown parameter required to calculate R is σ . It can be estimated comparing R predicted by the bubble model and R calculated from the lifetime of o-Ps in the bubble using the Tao-Eldrup model, given by Eq. (1). Nevertheless, the surface tension in the bubble is hardly the same as the macroscopic surface tension, e.g., in alkanes [40]. For the Sm- E phase of 6TCB, the surface tension obtained in this way at the atmospheric pressure $\sigma_{p \approx 0} = 61.5$ mN/m, is clearly larger than macroscopic surface tension $\sigma = (19-28)$ mN/m for liquid crystals in the smectic- A (Sm- A) phase reported in the literature [41]. However, the comparison of these values is not straightforward. It should be noticed that the Sm- A phase is a liquidlike phase in contrast to the Sm- E phase; hence, the lower value of the surfaces tension in comparison to the Sm- E phase should be expected. Moreover, for smectic liquid crystals, the surface tension is a tensor, and measured values are certain components of this tensor along the normal to a smectic layer.

The approximation used in the Tao-Eldrup model seems insufficient to calculate the change in the bubble size at high pressure because it was developed to estimate the relationship between the free volume radius and Ps lifetime and not the energy of Ps. Therefore, it is more accurate to calculate the Ps energy approximating the bubble with a finite square potential well of a spherical geometry and the depth U [42]. To consistently use the approximation of a finite well, the positron lifetimes corresponding to the bubble radii also are calculated by determining the shape of the Ps wave function

and the probability of finding Ps outside the potential well ($P_{\text{out}} = \int_R^\infty \psi^2 r^2 dr$, where R is the radius of the potential well and ψ is the Ps wave function). The potential depth $U = 1.45$ eV can be estimated by matching $\sigma_{p \approx 0}$ obtained from both approximations of the infinite and finite potential well. It can be compared with the value of U about 1.3 eV obtained by Zgardzińska and Goworek for the range of Ps bubble radii appearing in the experiments with liquid alkanes [40]. The dependence of the o-Ps lifetime on pressure for the potential depth $U = 1.45$ eV, is shown as the solid line in Fig. 9. The line follows the experimental points in the region of the Sm- E phase occurrence.

IV. CONCLUSIONS

The application of PALS to the study of the liquid crystalline Sm- E phase of 6TCB yields valuable information. The main results can be summarized as follows.

(i) In the Sm- E phase, Ps is created and annihilates in a layer of a lower electron density. This layer contains alkyl chains of molecules in a molten state. Their conformations change dynamically.

(ii) For 6TCB, the diameter of the o-Ps bubble is larger than for 4TCB. However, it is smaller than the thickness of the alkyl chain layer.

(iii) The temperature dependencies of the o-Ps component intensity for the supercooled Sm- E phase of 6TCB indicate glass softening and subsequent cold crystallization. The bond-lattice model (two-state glass transition model) explains the thermal activation of the centers where o-Ps is created and annihilates when the glass softens, however, in contrast to 4TCB the cold crystallization obscures this process.

(iv) Changes of the intensity of the o-Ps component during isothermal crystallization can be described by the Avrami equation with the Avrami exponent close to unity, which indicates low dimensional crystallization. However, the further decrease in the o-Ps lifetime points out that after the first stage of crystallization, the metastable phase M2 starts to transform into a more densely packed crystal phase.

(v) The decrease in the o-Ps lifetime and intensity for the pressure higher than 120 MPa may be attributed to the transition from the Sm- E phase to the metastable phase M1. There is a similarity to liquid n alkanes, where the application of pressure is equivalent to temperature lowering. Moreover, the equivalence relationship between pressure and temperature is also similar to that for n alkanes, which seems to confirm the presence of sublayers containing alkyl chains in a molten state.

(vi) The dependence of the o-Ps lifetime on pressure for the Sm- E phase may be described by the bubble model where the Ps bubble is approximated with a finite square potential well with the depth of $U = 1.45$ eV.

ACKNOWLEDGMENT

We wish to thank M. Tydda for his help with high-pressure PALS measurements.

- [1] S. Urban, K. Czupryński, R. Dąbrowski, J. Janik, H. Kresse, and H. Schmalfluss, *Liq. Cryst.* **28**, 691 (2001).
- [2] S. Urban, J. Czub, R. Dąbrowski, and H. Kresse, *Liq. Cryst.* **32**, 119 (2005).
- [3] S. Urban and A. Würflinger, *Phys. Rev. E* **72**, 021707 (2005).
- [4] S. Urban, J. Czub, R. Dąbrowski, and A. Würflinger, *Phase Trans.* **79**, 331 (2006).
- [5] M. Jasiurkowska, A. Budziak, J. Czub, M. Massalska-Arodź, and S. Urban, *Liq. Cryst.* **35**, 513 (2008).
- [6] R. Pełka, Y. Yamamura, M. Jasiurkowska, M. Massalska-Arodź, and K. Saito, *Liq. Cryst.* **35**, 179 (2008).
- [7] C. M. Roland, R. B. Bogoslovov, R. Casalini, A. R. Ellis, S. Bair, S. J. Rzoska, K. Czupryński, and S. Urban, *J. Chem. Phys.* **128**, 224506 (2008).
- [8] S. Urban and C. M. Roland, *J. Non-Crystal. Solids* **357**, 740 (2011).
- [9] M. Jasiurkowska, P. M. Zieliński, M. Massalska-Arodź, Y. Yamamura, and K. Saito, *J. Phys. Chem. B* **115**, 12327 (2011).
- [10] M. Jasiurkowska-Delaporte and M. Massalska-Arodź, *J. Mol. Liq.* **241**, 355 (2017).
- [11] K. Saito, T. Miyazawa, A. Fujiwara, M. Hishida, H. Saitoh, M. Massalska-Arodź, and Y. Yamamura, *J. Chem. Phys.* **139**, 114902 (2013).
- [12] T. Miyazawa, Y. Yamamura, M. Hishida, S. Nagatomo, M. Massalska-Arodź, and K. Saito, *J. Phys. Chem. B* **117**, 8293 (2013).
- [13] E. Dryzek, E. Juszyńska, R. Zaleski, B. Jasińska, M. Gorgol, and M. Massalska-Arodź, *Phys. Rev. E* **88**, 022504 (2013).
- [14] E. Dryzek and E. Juszyńska-Gałązka, *Phys. Rev. E* **93**, 022705 (2016).
- [15] Y. Yamamura, T. Adachi, T. Miyazawa, K. Horiuchi, M. Sumita, M. Massalska-Arodź, S. Urban, and K. Saito, *J. Phys. Chem. B* **116**, 9255 (2012).
- [16] T. Adachi, H. Saitoh, Y. Yamamura, M. Hishida, M. Ueda, S. Ito, and K. Saito, *Bull. Chem. Soc. Jpn.* **86**, 1022 (2013).
- [17] O. E. Mogensen, *Positron Annihilation in Chemistry* (Springer-Verlag, Berlin, 1995).
- [18] S. Pawlus, J. Bartoš, O. Šauša, J. Krištiak, and M. Paluch, *J. Chem. Phys.* **124**, 104505 (2006).
- [19] G. Dlubek, M. Q. Shaikh, K. Rätzke, F. Faupel, and M. Paluch, *Phys. Rev. E* **78**, 051505 (2008).
- [20] J. Bartoš, M. Iskrová-Miklošovičová, D. Cangialosi, A. Alegría, O. Šauša, H. Švajdlenkova, A. Arbe, J. Krištiak, and J. Colmenero, *J. Phys. Condens. Matter* **24**, 155104 (2012).
- [21] J. Bartoš, H. Švajdlenkova, Y. Yub, G. Dlubek, and R. Krause-Rehberg, *Chem., Phys. Lett.* **584**, 88 (2013).
- [22] J. Bartoš, G. A. Schwartz, O. Šauša, A. Alegría, J. Krištiak, and J. Colmenero, *J. Non-Cryst. Solids* **356**, 782 (2010).
- [23] C. A. Angell and K. J. Rao, *J. Chem. Phys.* **57**, 470 (1972).
- [24] S. Ishimaru, K. Saito, S. Ikeuchi, M. Massalska-Arodź, and W. Witko, *J. Phys. Chem. B* **109**, 10020 (2005).
- [25] Y. Yamamura, T. Murakoshi, M. Hishida, and K. Saito, *Phys. Chem. Chem. Phys.* **19**, 25518 (2017).
- [26] H. Iino and J. Hanna, *Polym. J.* **49**, 23 (2017).
- [27] S. Sugisawa and Y. Tabe, *Soft Matter* **12**, 3103 (2016).
- [28] T. Goworek, J. Wawryszczuk, and R. Zaleski, *Chem. Phys. Lett.* **402**, 367 (2005).
- [29] T. Goworek and B. Zgardzińska, *Acta Phys. Polon. A* **113**, 1379 (2008).
- [30] T. Goworek, R. Zaleski, and J. Wawryszczuk, *Chem. Phys.* **295**, 243 (2003).
- [31] J. Kansy, *Nucl. Instrum. Methods Phys. Res. Sect. A* **374**, 235 (1996).
- [32] S. J. Tao, *J. Chem. Phys.* **56**, 5499 (1972).
- [33] M. Eldrup, D. Lightbody, and J. N. Sherwood, *Chem. Phys.* **63**, 51 (1981).
- [34] R. A. Ferrell, *Phys. Rev.* **108**, 167 (1957).
- [35] G. Dlubek, M. Q. Shaikh, K. Rätzke, F. Faupel, J. Pionteck, and M. Paluch, *J. Chem. Phys.* **130**, 144906 (2009).
- [36] K. J. Rao, *Bull. Mater. Sci.* **1**, 181 (1979).
- [37] M. Jasiurkowska, Ph.D. thesis, Institute of Nuclear Physics PAN, Kraków, 2009.
- [38] B. Zgardzińska and T. Goworek, *Chem. Phys.* **405**, 32 (2012).
- [39] A. Würflinger and G. M. Schneider, *Ber. Bunsenges. Phys. Chem.* **77**, 121 (1973).
- [40] B. Zgardzińska and T. Goworek, *Chem. Phys.* **411**, 1 (2013).
- [41] H. Schüring, C. Thieme, and R. Stannarius, *Liq. Cryst.* **28**, 241 (2001).
- [42] H. Nakanishi and Y. C. Jean, in *Positron and Positronium Chemistry*, edited by D. M. Schrader and Y. C. Jean (Elsevier, Amsterdam, 1988), pp. 169–173.